De novo peptides that induce the liquid-liquid phase separation of α-synuclein

Tatsuya Ikenoue (t-ikenoue@g.ecc.u-tokyo.ac.jp)
Department of Chemistry, The University of Tokyo, Tokyo, Japan https://orcid.org/0000-0002-7271-1894

Masatomo So
Department of Future Basic Medicine, Nara Medical University, Nara, Japan

Naohiro Terasaka
Department of Chemistry, The University of Tokyo, Tokyo, Japan

Wei-En Huang
Department of Chemistry, The University of Tokyo, Tokyo, Japan

Yasushi Kawata
Department of Chemistry and Biotechnology, Tottori University, Tottori, Japan

Yohei Miyanoiri
Institute for Protein Research, Osaka University, Osaka, Japan

Hiroaki Suga (hsuga@g.ecc.u-tokyo.ac.jp)
Department of Chemistry, The University of Tokyo, Tokyo, Japan https://orcid.org/0000-0002-5298-9186

Research Article

Keywords: alpha-synuclein, liquid-liquid phase separation, peptide, Parkinson's disease, RaPID screening

Posted Date: April 18th, 2023

DOI: https://doi.org/10.21203/rs.3.rs-2112220/v1

Abstract

Liquid-liquid phase separation (LLPS) of protein that leads to formation of membrane-less organelles is a critical event to many processes in the cell. Recently, some disease-related proteins, such as α-synuclein (αSyn), were found to undergo LLPS before their formation of amyloid fibrils. However, the progress towards controlling LLPS has been limited, and there has been no emerging engineered de novo molecules to induce and modulate the LLPS of targeted proteins. Here we report peptides that efficiently induce the LLPS of αSyn, discovered by the RaPID (random non-standard peptides integrated discovery) system. These peptides are able to co-localize with αSyn in liquid droplets via heterotypic interacting with the N- and C-terminal regions of αSyn. Our study demonstrates the capacity of target-specific peptides to control LLPS and modulate the physical nature of condensate. Thus, these peptides could be a unique tool to gain deeper insights in the LLPS-mediated amyloid formation.

Introduction

Liquid-liquid phase separation (LLPS) of proteins accompanies the formation of condensed liquid droplet phase, and such phenomena result in a wide variety of cellular functions and regulations[1–3]. However, these membrane-less organelles can also pose a risk for the formation of amyloid fibrils, which potentially lead to serious neurodegenerative diseases. Condensates of intrinsically disordered proteins (IDPs), such as fused in sarcoma (FUS) and Tau, or proteins bearing an intrinsically disordered region (IDR) such as hnRNPA1, have been shown to undergo LLPS and subsequently form fibrils through a process known as liquid-to-solid phase transition[4–9]. These IDPs and IDRs, which are often highly charged and flexible, induce LLPS by forming weak, transient multivalent interactions between protein-protein and protein-RNA, contributing to the dynamic nature of phase separated compartments[3,10–12].

Diseases associated with protein aggregations are likely developed or progressed due to a failure to maintain homeostasis in the living systems. The aggregation of proteins from a native (or soluble) state to an amyloid state may generally proceed through an intermediate condensate that is typically metastable[13,14]. Therefore, the liquid droplet of amyloidogenic proteins can be a potential therapeutic target; i.e., controlling the physical nature and subsequent liquid-to-solid phase transition can be a relevant strategy to modulate the disease-associated aggregation. However, there is little understanding how we can change the phase behavior and fluidity of droplets at the molecular level. Several methods have been designed to incorporate protein into phase-separated liquid droplets using molecular fusions consisting of two protein components[15–18]. For example, protein, large domain, or engineered polypeptide inspired from native protein known as major components of homotypic LLPS in the cell, such as FUS (~ 75 kDa), have been combined with functional proteins or fluorescent proteins. However, to our knowledge, a target-specific *de novo* molecule inducing LLPS has not yet been reported in the literature, even though such molecules have potentials for a wide range of applications to LLPS studies, such as drug partition in condensates of target protein and formation of artificial organelle of non-LLPS-inducing proteins without interfering with natively existing condensates in the cell system. These applications hold a

substantial promise for challenging indications, which may allow modification of IDPs and IDRs currently considered undruggable with small molecules[19,20].

Alpha-synuclein (αSyn) is an amyloidogenic IDP involved in Parkinson's disease[21–25], and recent reports suggest that it also undergoes LLPS through primarily hydrophobic interactions, although this process requires certain purification methods and atypical long incubation times[26,27]. The monomeric form of αSyn is intrinsically disordered and lacks a permanent structure, consisting of three characteristic domains, consisting of the N-terminal region with many charged residues, the hydrophobic region called 'non-amyloid-β component' (NAC), and the negatively charged C-terminal region. Because of this dynamic feature of αSyn, it is difficult to identify the molecular species that may lead to a conventional enthalpy-focused mechanism of binding, as similarly shown for amyloid-β[28–30]. NMR and cryo-EM studies have recently revealed a highly ordered structure of the fibril core of αSyn, despite the regions of the N-terminus (1–37 residues) and C-terminus (98–140 residues) not being well-defined[31–33]. This observation suggests that the dense disordered tails are surrounded by the structured fibril core.

Various strategies are currently available for the discovery of cyclic peptides against given targets. The random non-standard peptides integrated discovery (RaPID) system[34] (Fig. 1a) uses the combination of messenger RNA display[35] and genetic code reprogramming facilitated by the flexible in vitro translation, referred to as FIT, system[36]. This system enables the ribosomal synthesis of extremely large ($> 10^{12}$) libraries of natural product-like macrocyclic peptides and rapid selection based on binding to protein targets of interest. Even though we witnessed many successful discoveries of various types of proteins, including enzymes, membrane proteins, secreted proteins, and intracellular proteins involving in protein-protein interaction, we have not yet tried selecting macrocyclic peptides against a IDP or IDR that self-aggregates. Since the conformationally restrained structure of macrocyclic peptides would lead to a relatively small entropy cost upon binding and achieve remarkable binding affinity and specificity[37–39], we envision that this approach may yield adequate macrocycles capable of interacting the disordered region of protein.

Here we report *de novo* peptides that induce the LLPS of αSyn in vitro. Five out of seven selected peptides from the RaPID screening were able to induce LLPS of αSyn. NMR studies on the αSyn have allowed us to propose a mechanism where the interactions of a peptide, **FD1**, with the N- and C-terminal regions of αSyn could drive the formation of droplets. By monitoring the fluidity of αSyn droplets, we demonstrate the capacity of the peptide and its mutant to modulate the physical nature of induced droplets and following liquid-to-solid phase transition of αSyn condensate. These peptides will be a promising tool for fundamental studies of αSyn LLPS and may provide invaluable information on how the LLPS-mediate fibril formation of disease-related proteins can be regulated.

Results

RaPID selection of macrocyclic peptides against fibril states of αSyn

In order to obtain peptides which can induce the LLPS of αSyn, we performed selection by means of the RaPID system using αSyn amyloid fibrils as a displaying target (Fig. 1a). As discussed earlier, recent structural studies on αSyn revealed that ~ 40 residues in both N- and C-termini of αSyn are flexible and surround the core of the fibril with a dense mesh of disordered regions (Fig. 1b), described as 'fuzzy coat'[40]. Therefore, screening against the fibril state of αSyn with aligned disordered regions at narrow intervals (~ 4.8 Å) possibly identifies peptides that can form interaction bridging multiple αSyn molecules and result in an induction of LLPS of αSyn.

A puromycin-ligated mRNA library was constructed to encode macrocyclic peptides with *N*-chloroacetyl-L-Tyrosine (^{L}Y-library) or *N*-chloroacetyl-D-Tyrosine (^{D}Y-library) as an initiator, followed by a random peptide region consisting of 6–15 residues, a cysteine, and ending with a short linker peptide. Upon translation of the mRNA library, each mRNA template was ligated to the C-terminus of the cognate linear peptide to form mRNA-peptide fusion via the puromycin linker, and then cDNA synthesis was performed by reverse transcription (RT). During the RT step at 42°C, the N-terminal chloroacetyl group completely cyclized with its downstream cysteine to form a thioether-macrocyclic peptide (note that some species spontaneously cyclized during other manipulation steps, *e.g.* EDTA-dissociation of the mRNA-peptide fusion from ribosome). Each library was applied to the protein-free magnetic beads to remove background nonspecific binders, and then to the αSyn fibril-immobilized magnetic beads to enrich specific binders to the fibril state of αSyn. The morphology of the amyloid fibrils, which were used for the RaPID campaign, was determined by AFM, giving the height of 9.0 nm and periodic twisting pitch of 99 nm (Fig. 1c, **Supplemental method**). This observation was consistent with previously reported structural analysis using cryo-EM[32].

After seven rounds of the RaPID selection, both ^{L}Y-library and ^{D}Y-library yielded a successful enrichment of active species selectively bound to the immobilized αSyn fibrils over the background. Sequence alignment analysis of the enriched species in libraries of the 7th rounds revealed that three and five converged classes of macrocyclic peptides were converged in the ^{L}Y-library and ^{D}Y-library, respectively. Since mRNA fused to each peptide in principle increase their water solubility, for the naked macrocyclic peptides of **FL2–3** and **FD1–5**, we modified their C-terminus with a short solubility tag GKKK-NH_2 (Fig. 1d). Note that we decided to exclude **FL1** for further studies due to its extremely low theoretical score of water solubility even though it was most enriched with the form of its mRNA fusion.

To evaluate the binding affinity and binding mode, the selected peptides were chemically synthesized, and Isothermal calorimetry (ITC) measurements were performed (**Supplementary Fig. 1**). The dissociation constant K_D for the αSyn fibrils was a single digit micromolar range of affinity and the binding ratio (n value, peptide/αSyn) displays sufficiently lower than 1.0 (Fig. 1d), implying that **FL2–3**, and **FD1–3** likely

interact with multiple αSyn molecules in a bridging manner. On the other hand, though **FD4** and **FD5** also showed a similar range of K_D values, the binding ratio n value was close or above 1.0.

Selected Peptides Efficiently Induced Droplet Formation Of αsyn

In order to investigate whether the selected peptides can generate liquid droplets with αSyn, 100 μM of αSyn was mixed with 2 molar equivalents of peptides in 20 mM sodium phosphate buffer (NaPi) (pH 7.5) with 10% polyethylene glycol (PEG)-8000, which often used as a molecular crowder. After incubating on ice for 1 h, Differential interference contrast (DIC) images of the solution showed many spherical droplets in the bulk in the presence of **FL2–3** and **FD1–3**, whereas a **FD4** and **FD5** showed aggregation-like assemblies (Fig. 2a). For comparison, we synthesized and tested a cationic peptide Tyr-$(Lys)_{19}$-NH_2 (**polyK**), where the N-terminal Tyr was incorporated for the purpose of determination of its concentration. In recent studies, it was shown that αSyn could form droplets with prion protein via electrostatic interaction between the positively charged N-terminal segment of prion and the negatively charged C-terminus region of αSyn[41]. Moreover, poly-L-Lys could form droplets with ssDNA[42] or nucleotides[43–46] with stoichiometric charge neutralization. In our experiments, although two molar equivalents of **polyK** could induce LLPS of αSyn, the total amount of droplets was much lower than that induced by **FL2–3**, and **FD1–3**. These observations suggest that not only the positively charged amino acids but also the other amino acids in the peptide sequence are important for the efficient LLPS of αSyn.

Based on the consideration of the abundance in sequence population generally reflecting to the binding potency as well as the high ‘theoretical’ score of water solubility, we have chosen two peptides, **FL2** and **FD1**, for further experiments. The formation of droplets of sizes as well as amounts was dependent on the peptide (10–1,000 μM) as well as αSyn (20–200 μM) concentrations (Fig. 2b). Quantitative turbidity measurements were also demonstrated at various concentrations of the peptides with 100 μM αSyn, being well consistent with a concentration-dependent increase in the amount of droplets (Fig. 2c). The generated droplets showed liquid-like properties, as represented by their adsorption onto the glass plate surface (Fig. 2d, **Supplementary Movie 1**) and fusion events of droplets (Fig. 2e, **Supplementary Movie 1**) were observed by DIC and time-lapse fluorescence microscopy. Temperature-dependent turbidimetry showed that the condensates were dissociated to a dispersed monomeric state as the temperature increased, and a reversibility of the formation of droplets was also verified by regenerating droplets after heat dissociation by jumping the temperature to 20°C (**Supplementary Fig. 2**). Such a reversibility of the assembly is a characteristic nature of liquid droplets, which should not be observed in stable solid aggregates. The phase diagram of αSyn at a different incubation time (1 h or 1 day at 4°C) was constructed by judging from the shape of assemblies in DIC images (**Supplementary Fig. 3**), classifying monomers, droplets, aggregates, and gel states. To confirm whether droplets contain both αSyn and peptides, we performed two-color confocal fluorescence imaging using 1% rhodamine-labeled αSyn (αSyn-Rhod; [αSyn]:[αSyn-Rhod] = 99:1) and 1% fluorescein-labelled peptides (FL2C-Fluor and FD1C-Fluor). Their fluorescence images showed that both αSyn and peptides localized together into the droplet phase (Fig. 2f, **Supplementary Fig. 4a, b**).

To verify the specificity of amino acid sequence of **FL2** and **FD1**, we tested sequence-scrambled peptides (**$FL2_{scr}$** and **$FD1_{scr}$**) and determined their LLPS efficiency (**Supplementary Fig. 5**). In fact, **$FL2_{scr}$** and **$FD1_{scr}$** did not induce LLPS but rather suppressed, indicating that the selected sequences of **FL2** and **FD1** are needed to interact with αSyn and induce LLPS. To investigate the effects of cyclic scaffold of **FL2** and **FD1**, we confirmed the LLPS-inducing ability of their non-cyclic forms, $FL2_{linear}$ and $FD1_{linear}$, respectively (**Supplementary Fig. 6a**). The linear peptides did not exhibit significant changes in their LLPS-inducing ability in the absence and presence of DTT (**Supplementary Fig. 6b**). To gain insights into the dynamics of the droplets, we tested whether the droplets allow protein-size molecules conjugated with the $FL2_{linear}$ and $FD1_{linear}$ to be co-localized. We used sfGFP as a model protein, and the fluorescence images demonstrated that both sfGFP-labeled $FL2_{Linear}$ ($FL2_{Linear}$-sfGFP) and sfGFP-labeled $FD1_{Linear}$ ($FD1_{Linear}$-sfGFP) co-localized uniformly with αSyn in the droplet phase (**Supplementary Fig. 6c-e**).

Interactions Responsible For Llps Of αsyn And Peptides

To determine an interacting region(s) in αSyn responsible for LLPS induced by FL2 and FD1, we performed ^{1}H-^{15}N heteronuclear single quantum coherence (HSQC) experiments at 5°C with 100 μM of ^{15}N-labeled αSyn in the presence and absence of **FL2** and **FD1**. The presence of FL2 did not cause a major chemical shift perturbation (Δδ) in the HSQC spectra likely due to precipitation and adsorption of the large αSyn droplets onto the bottom of the NMR tube (**Supplementary Fig. 7a-d**). In contrast, the HSQC spectra in the presence of **FD1** showed significant chemical shift perturbation (Δδ) at the C-terminal region of αSyn (Fig. 3a, b, **Supplementary Fig. 7e**) as well as their peak intensities ($I_{+\,FD1}/I_{-\,FD1}$) were slightly decreased (Fig. 3b). We further performed paramagnetic relaxation enhancement (PRE) measurements to detect a transient long-range interaction using **FD1** labelled with a paramagnetic spin-label, (1-oxyl-2,2,5,5-tetramethylpyrrolidin-3-yl)methyl methanethiosulfonate (MTSL), referred to as **FD1**-C21R1. The result showed a dramatic decrease in cross-peak intensity at the C-terminal region of αSyn (Fig. 3c). Interestingly, the observed intensity at the N-terminal region also showed a decrease in the presence of **FD1**-C21R1. This observation suggested that **FD1** can also bind to the N-terminal region of αSyn and/or that intramolecular interaction between the N- and C-terminal regions of αSyn was accompanied by **FD1** and form a compact structure[47].

Since these results of NMR experiments suggested the importance of electrostatic interaction via highly charged N- and C-terminal regions of αSyn for LLPS, we further tested the effect of salt on LLPS. The DIC images and the turbidity of solutions clearly showed a decrease in the total amount of droplets as the NaCl concentration was increased (0–200 mM) (Fig. 3d). Although αSyn solutions with PBS, which contains 140 mM of NaCl, showed less droplet formation, droplet can still be formed by increasing the peptide concentration (**Supplementary Fig. 8**). We also tested the LLPS induction efficiency of **$FL2_{NoTag}$** lacking the short solubility-tag of triple Ks of FL2, revealing that the deletion of solubility-tag did not lose their efficiency of LLPS induction at 0.2–1.0 molar equivalent (**Supplementary Fig. 9**). This indicates that the residues in the body sequence of peptides identified by the selection campaign contribute to the

observed LLPS of αSyn. To confirm whether the N- and/or C-terminal regions of αSyn are required to droplet formation, we prepared truncated αSyn constructs at the C-terminal region ($αSyn_{1-103}$) and N-terminal region ($αSyn_{104-140}$) and examined their LLPS efficiency with **FL2** and **FD1** (Fig. 3e). The results clearly show that neither truncated αSyn efficiently yields LLPS compared with the full-length αSyn. Most strikingly, $αSyn_{1-103}$ with **FL2** formed aggregates rather than liquid droplets, whereas that with **FD1** completely lost the ability to form neither liquid droplets nor aggregates. Interestingly, when the mixture of $αSyn_{1-103}$ and $αSyn_{104-140}$ was used with the peptides, LLPS induction could not be recovered. This suggests that heterotypic interaction with the N- and C-terminal regions on the identical αSyn molecule may be required for such efficient LLPS events.

Liquidity Of Droplet Induced By Fl2 And Fd1

In order to gain more insights into how we can control the dynamic properties of the induced liquid droplets, we investigated the dynamic properties of the liquid droplets of αSyn induced by the peptides. The internal mobility of the droplets composed of αSyn and each peptide was measured with fluorescence recovery after photobleaching (FRAP) technique using the rhodamine-labelled αSyn (αSyn-Rhod) (Fig. 4). The αSyn-Rhod in droplets formed at a concentration of 200 μM FL2 with NaPi showed an approximately 65% fluorescence recovery and remained high molecular mobility even after 1 h incubation (Fig. 4a, b). Droplets formed at various **FL2** concentrations showed a concentration-dependent change in the fluorescence recovery with local minima at 500 μM (Fig. 4c). Their measurements in PBS buffer also showed high fluorescence recovery rates (**Supplementary Fig. 10a**). On the other hand, droplet induced by 200 μM **FD1** showed an approximately 94% αSyn-Rhod fluorescence recovery after 2 min incubation and a liquid-like property declined in an incubation-time-dependent manner (approximately 8% fluorescence recovery at 1 h incubation). These findings demonstrate that the liquid droplets induced by **FD1** undergo maturation to a solid state. Whereas 1 h incubation with FD1 at room temperature significantly decreased the fluorescence recovery, that on ice showed high fluorescence recovery (**Supplementary Fig. 10b**), indicating that the lowering temperature delays the maturation (aging) of liquid droplets to a solid state. Taken together, we have shown that the liquidity of formed condensate of αSyn is modulated by peptide concentrations. Moreover, αSyn droplets induced by **FL2** and **FD1** showed different maturation propensities, where **FD1** represented a liquid-to-solid phase transition of αSyn within 1 h, while **FL2** kept the liquidity of αSyn for at least 1 h.

Aggregation Of αsyn Via Llps Modulated By Fl2 And Fd1

LLPS-mediated liquid-to-solid phase transitions into pathological aggregates have been reported for various IDPs or IDRs[7,48,49]. αSyn accumulation in the brain have been observed with co-aggregation with other pathological species such as tau in Lewy body[50,51] and prion protein in early cytoplasmic inclusions bodies[52]. Multi-component colocalization with other interacting partners may be generated by synergistic interactions in cell bodies. Indeed, αSyn can form liquid droplets with prion protein, and their

interaction promotes amyloid fibril formation[41]. Therefore, we next explored how LLPS induced by the αSyn-peptide heterotypic interactions could affect the fibril formation of αSyn (Fig. 5). We performed the kinetic analysis of αSyn aggregation under three characteristic conditions: (i) the conditions where αSyn does not form condensates (without PEG in PBS buffer), (ii) the conditions where αSyn forms condensates only at high peptide concentrations, *i.e.* a middle LLPS tendency (10% PEG in PBS buffer), and (iii) the conditions where αSyn forms condensates even at low peptide concentrations, *i.e.* a high LLPS tendency (10% PEG in NaPi buffer). We monitored the fibril formation of αSyn under these conditions (i–iii) in the absence and presence of peptides (from 0.1 to 10 molar equivalent) using the fluorescence of thioflavin T (ThT) as an amyloid-sensitive probe[53,54] (Fig. 5a). Comparisons of the lag-time $t_{1/2}$ at various concentrations of **FL2** and **FD1** are summarized in Fig. 5b. The results obtained under the (i) conditions indicated both **FL2** and **FD1** showed no acceleration of the fibril formation of αSyn, but rather expand the lag-time derived from a time to reach a half maximum intensity ($t_{1/2}$) (Fig. 5a, b). On the other hand, the observed ThT profiles under the (ii) conditions showed a decrease in the ThT intensity along with lag-time changes; and those under the (iii) conditions indicated a large acceleration of αSyn aggregation with intensity changes. Taken together, the increasing LLPS tendency of αSyn with **FL2** and **FD1** likely accelerates amyloid fibril formation.

The liquid-to-solid phase transitions of droplets have been classified into two types: amyloid fibril formation and non-amyloidogenic aggregation. Non-amyloidogenic aggregation, e.g. amorphous aggregation, is formed without a lag time; therefore, it generally competes with the slow nucleation-dependent amyloid formation. To monitor the formation of non-fibrillar aggregates of αSyn, the fluorescence of 8-anilino-1-naphthalenesulfonic acid (ANS), often used as a probe for amorphous aggregates, was measured simultaneously with ThT. Prior to this experiment, we first confirmed the ANS was incorporated into the liquid droplets and showed fluorescence as time passes (Fig. 5c). The ANS profiles monitored at the (ii, iii) conditions indicated an early appearance of hydrophobic assemblies within the initial 10 h (Fig. 5d, **Supplementary Fig. 11a**). The ThT profiles, however, did not show any increase until at least 10 h, showing that the early assemblies do not yet have a fibrillar structure. The fluorescence images showed morphological changes from needle-like fibrils to noodle-like fibrils in the presence of **FL2** and **FD1** (Fig. 5e). These morphological changes induced by **FL2** and **FD1** explain the decrease of magnitude of ThT signal and increase of ANS intensity at high concentrations of **FL2** and **FD1** (Fig. 5f, **Supplementary Fig. 11b**).

Discussion

Various peptide-based LLPS, such as peptide-peptide and peptide-nucleic acids condensates, have been reported previously[55]. The peptides reported to date can be divided into two types: mimic peptides, which contain amino acids homologous to self-assembling proteins, and simplified polyelectrolytes peptides, such as poly-lysine or poly-arginine, whose electronic interactions are their main driving force. In this work, we successfully identified *de novo* macrocyclic peptides that induce LLPS of αSyn by means of the RaPID system. We have considered that peptides which have multiple interactions with αSyn could be

screened by displaying the fibril state of αSyn. Indeed, five out of seven identified peptides indicated low molar binding ratio to αSyn, and they induced LLPS of αSyn. The selected peptides, **FL2** and **FD1**, efficiently induced αSyn LLPS in a concentration-dependent manner without a lag-phase, whereas αSyn alone did not form LLPS at least within a day. Despite the high prevalence of disordered proteins in human disease[56–59], no clinically approved drug directly targets disordered proteins in their monomeric forms[28,60,61]. Here, the condensates induced by the selected peptides showed a dynamic, liquid-like nature. We also demonstrated that small compounds and proteins, such as fluorescein and sfGFP, can be incorporated into the liquid droplets by conjugating them with **FL2** and **FD1**, as well as their linearized form. This ability of the peptides to co-localize the conjugated clients into the dynamic condensed phase of the target suggests a potential application: drug- or enzyme-conjugation with these peptides can efficiently promote their reaction activity in the droplets, as suggested in cancer therapeutics in nuclear condensates or in enhancing enzyme activity in cells[62,63]. The interaction specificity was proved to a certain extent by comparison with polyK, scrambled **FL2** and **FD1**, and solubility-tag-truncated **FL2**. Further optimization of peptide affinity and specificity may be needed to avoid competitive protein-protein and protein-RNA interactions in the cell system. The optimization of peptides could be advantageously achieved through display-facilitated deep mutational scanning, as reported elsewhere[64].

The NMR studies on the condensed αSyn revealed that **FD1** mainly interacts with the C-terminal region of αSyn via electrostatic interactions. The disordered C-terminal region of αSyn has been predicted to have a high droplet-promoting propensity by well-known LLPS predictor FuzDrop[65] (**Supplementary Fig. 12a**). The residues Q2, R3, K6, R8, R11, T13, C14 and C16 in **FL2** and the H5, K6, Q12, R14, and S15 in **FD1** may be principal drivers of electrostatic interactions and dipole-dipole interactions with the C-terminal region of αSyn (residues 99–140), which contains 15 anionic residues and 5 polar residues. Because the HSQC spectra showed significant chemical shift perturbation (Δδ) at Y133, and Y136 in αSyn, π-π interactions and cation-π interactions may also contribute to the LLPS. Furthermore, the PRE measurements indicated that **FD1** also weakly interacts with the N-terminal region of αSyn, which has been predicted to have an intermediate droplet-promoting propensity by FuzDrop. Since the aromatic residues are abundantly present in the **FD1** sequence (Y1, W4, W8, F9, and Y12) and the other four LLPS-inducing-peptides also contain 5–7 aromatic residues in the 14–16 amino acid sequences, cation-π interaction between aromatic residues in peptides and the 11 cationic residues on the N-terminal region of αSyn may also contribute to the interaction specificity and the LLPS efficiency of αSyn. Indeed, we revealed the critical role of both N- and C-terminal regions of αSyn on the two-component LLPS by using deletion mutants. Peptide interactions to the N- and C-terminal regions of αSyn also support that the RaPID system successfully screened macrocycles against the displayed fuzzy coats of αSyn fibrils. Based on the interaction analysis, we propose a naive hypothetical mechanism for the induction of LLPS of αSyn by **FL2** and **FD1** as follows (Fig. 6). In the monomeric state of αSyn, the long-range intramolecular interaction between charged N- and C-terminal regions has led to a compact form of αSyn and maintain its solubility[47,66–68]. The interaction of **FL2** and **FD1** with the N- and/or C-terminal regions of αSyn may shield the intramolecular interactions and lead to the opened state of αSyn, which is preferred to form interaction network. Furthermore, since the peptides were identified by screening against the fibril state of

αSyn with a dense mesh of the N- and/or C-terminal regions, the macrocycles may form multivalent interactions that bridge multiple αSyn molecules. In addition to such promotion of LLPS, the structural modification of αSyn monomers to an opened state might contribute to an acceleration of fibril formation, where the exposed NAC region has high amyloid propensity, as predicted by Zyggregator[69] (**Supplementary Fig. 12b**), and a N-terminal segment of αSyn (residues 36–42) is required for aggregation[47].

Recently, many proteins in human proteome have been reported to be involved LLPS as shown in public databases such as PhaSepDB[70], PhaSePro[71], and LLPSDB[72,73]. Using these datasets, the FuzDrop method has predicted that about 80% of these proteins can act as droplet clients, which form condensates via sequence-dependent interactions with suitable partners[65]. Although single-component LLPS of αSyn has also been reported, it indicated different interacting regions of the condensed αSyn: the N-terminal and NAC regions[26]. Since the single-component LLPS is promoted by an increase in salt concentrations, αSyn alone may undergo homotypic LLPS primarily via hydrophobic interaction. On the other hand, the prediction of LLPS-driving potential using the FuzDrop method agrees very well with the interacting regions of the two-component heterotypic LLPS induced by **FD1**. Therefore, the peptides interacting with highly LLPS-prone regions have the potential to serve as superior modulators of LLPS and subsequent liquid-to-solid phase transition (LSPT).

The concentration effect of molecules via LLPS can lead to a metastable supersaturated state of protein, and it often precedes before the formation of more stable amyloid fibrils[6,26,74,75]. Thus, a step-by-step formation of fibrillar aggregates in the condensates seems to be general as defined by Ostwald's rule of stages, according to which the morphologies of crystals change over time, guided by their kinetic accessibility and thermodynamic stabilities[14,76]. Therefore, the liquid droplets of amyloidogenic proteins, which might be an initial stage of amyloid formation, can be a potential target for therapeutics. In this study, we demonstrated the capacity of **FL2** and **FD1** to modulate the dynamic properties of the αSyn condensates and their LSPT. The aggregation assay indicated that the liquid droplets induced by **FL2** and **FD1** clearly showed a phase transition to non-amyloidogenic aggregates in the lag-phase of αSyn fibrillation. Although the acceleration of the amyloid fibril formation was accompanied by LLPS-induction, the rapid formation of competitive non-fibrillar aggregated species might result in a reduction of the mass of pathological aggregates and can offer opportunities for suppressing their toxicity. Our novel LLPS-inducing and LSPT-modulating peptides would become a promising tool for fundamental investigations of the LLPS and for the therapeutic interventions of amyloid diseases.

Materials And Methods

Recombinant expression and purification of αSyn

The plasmid that expresses human αSyn and the mutants were amplified as previously described[77]. αSyn, $αSyn_{1-103}$, and $αSyn_{104-140}$ were expressed in an *Escherichia coli* BL21(DE3) transformed by pET-

αSyn[77] in 2 L flasks at 37°C with 1 L of Luria-Bertani (LB) medium. Isotopically labeled ^{15}N-αSyn were expressed in 2 L flasks at 37°C with 1 L of minimal M9 batch medium. Cells were suspended in purification buffer (50 mM Tris-HCl, pH 7.5, containing 1 mM EDTA and 0.1 mM dithiothreitol), disrupted using sonication, and centrifuged (10,000×*g*, 30 min). Streptomycin sulfate (final 5%) was added to the supernatant to remove nucleic acids. After removal of nucleic acids by centrifugation, the supernatant was heated to 80°C for 30 min and then centrifuged. In this step α-synuclein remained in the supernatant. The supernatant was precipitated by the addition of solid ammonium sulfate to 70% saturation, centrifuged, and dialyzed overnight and then applied onto a HiTrap-Q column (cytiva) with 50 mM Tris-HCl buffer, pH 7.5, containing 1 mM EDTA and 0.1 mM dithiothreitol as running buffer. Samples were eluted with a linear gradient of 0–1 M NaCl. Collected fractions were dialyzed overnight and then applied onto a reversed-phase HPLC (RP-HPLC), using a Prominence HPLC system (Shimadzu) under linear gradient conditions. Mobile phase A (comprising water with 0.1% TFA) was mixed with mobile phase B (0.1% TFA in acetonitrile). Purified peptides were lyophilized, and molecular mass was confirmed by matrix-assisted laser desorption/ionization time-of-flight mass spectroscopy (MALDI MS), using an UltrafleXtreme instrument (Bruker Daltonics).

αsyn Fibrils For Selection

Since polymorphism is a characteristic property of amyloid fibrils[78], it is important to prepare and apply homogeneous fibril for the RaPID screening. We first amplified specific αSyn fibril by repeating seeding experiment. Solutions of monomeric αSyn were prepared by dissolving the lyophilized αSyn with PBS buffer. Solutions were filtered using a 0.22 μm PVDF filter, and the αSyn concentration was determined by NanoDrop using ε_{280} = 5120 L mol^{-1} cm^{-1}. Seeding experiments were performed by adding 5% (v/v) preformed fibrils to 100 μM monomeric αSyn solution. First generation of fibrils for seeding experiments were prepared by spontaneous fibril formation by monitoring ThT fluorescence. Assays were initiated by placing the 96-well plate at 37°C with a cycle of 3 min shaking and 27 min quiescence in a plate reader (Flex station; Molecular Devices). Preformed fibrils were well fragmented by ultrasonication before seeding, and the seeded solution was incubated at 37°C for 1 week. This seeding experiment was repeated six times with PBS buffer at pH 7.5. The homogeneity of the morphology of the 7th generation of amyloid fibrils was confirmed by analyzing 10 AFM images. We thus decided to use this particular sample for our RaPID campaign.In order to immobilize the fibrils on Dynabeads, human $(His)_6$-αSyn (Wako Pure Chemical Industries Ltd) was attached to fibril ends in an amyloid propagation manner by adding 5% of $(His)_6$-αSyn to the 7th generation of fibrils.

Atomic Force Microscopy

Conventional atomic force microscope (AFM) measurements were performed in air with the sample deposited on a cleaved bare mica substrate. To detect small assemblies in Fig. 4, the mica surface was functionalized. The mica substrate was incubated with a 10 μl drop of 0.05% (v/v) APTES ((3-

Aminopropyl)triethoxysilane, Fluka) in Milli-Q water for 1 min at room temperature, rinsed with ultrapure water, and then dried by airflow. The preparation of the mica AFM samples was realized at room temperature by deposition of a 10 µl aliquot of 10 µM solution of 7th generation αSyn fibrils for 10 min. Then, the sample was rinsed with ultrapure water and dried by a gentle flow of air. Imaging was performed in tapping mode on a Bruker Multimode-8A AFM with 0.9 Hz line-rate for 5 by 5 µm images.

Selection Of Anti-α-syn-fibril Peptides

The random mRNA library and the two non-canonical aminoacyl-transfer RNAs, ClAc-lTyr-tRNA$^{fMet}_{CAU}$ and ClAc-d-Tyr-tRNA$^{fMet}_{CAU}$ were prepared as previously reported[79]. Briefly, 40 µM tRNA$^{fMet}_{CAU}$, 600 mM $MgCl_2$ and 5 mM ClAc-l-Tyr-CME or ClAc-d-Tyr-CME in dimethylsulfoxide (DMSO) were mixed in 100 mM HEPES-KOH (pH 8.0) and incubated on ice for 1 h. After the reaction, one-tenth of a volume of 3 M sodium acetate (pH 5.2) was added and the RNA was ethanol precipitated. The pellet was rinsed with 70% (v/v) ethanol containing 0.1 M sodium acetate (pH 5.2), then 70% ethanol only. The pellet was air dried and dissolved in 1 mM sodium acetate (pH 5.2) before use. Thioether macrocycles targeting human αSyn monomers were selected using the RaPID system[34,79], slightly modified as follows: 1 µM mRNA library was incubated with 1.5 µM puromycin linker in the presence of T4 RNA ligase for 30 min at 25°C and was purified by phenol–chloroform extraction and ethanol precipitation. To generate the respective peptide library initiated with ClAc-l-Tyr (L-library) or ClAc-d-Tyr (D-library), 1.4 µM mRNA–puromycin library was translated in a methionine-deficient FIT system[36] at a scale of 150 µl total volume in the presence of 50 µM ClAc-l-Tyr-tRNA$^{fMet}_{CAU}$ or ClAc-d-Tyr-tRNA$^{fMet}_{CAU}$ for 30 min at 37°C. After a 12-min incubation at 25°C, the temperature was elevated to 37°C and maintained for 30 min, to promote macrocyclization. The fused macrocycle–mRNA was subsequently reverse transcribed by RQ-RTase (Promega) for 1 h at 42°C. The reverse-transcribed peptide-mRNA fusions were split into four 70.5 µL aliquots and each was buffer-exchanged through a small column (1 mL) of TBST-equilibrated Sephadex G25 (GE Healthcare) via centrifugation at 800 × *g* for 1 min. The buffer-exchanged peptide-mRNA fusions were collected and 282.9 µL of blocking buffer (TBST containing 0.2% acetylated BSA; Life Technologies) was added. A 0.5 µL aliquot of the peptide-mRNA fusions was taken from the mixture and saved for the determination of the total amount of inputted mRNA. The peptide-oligonucleotides (mRNA/cDNA) fusions were then incubated with Dynabeads His-tag isolation and pulldown (invitrogen) for 30 min at room temperature (negative selection against beads). The unbound fraction was then incubated with human αSyn fibrils immobilized on Dynabeads for 30 min. αSyn fibrils were masked with 2 mg/mL yeast tRNA (invitrogen) in advance of applying the library. During selection, αSyn fibrils were treated at room temperature to avoid cold denaturation[80]. The resultant complementary DNAs were eluted by mixing with 1 × PCR reaction buffer and heating at 95°C for 5 min, followed by immediate separation of the supernatant from the beads. A small fraction of the cDNA was allocated to real-time PCR quantification using a LightCycler 2.0 (Roche); the remainder was amplified by PCR. The resulting duplex DNAs were purified by phenol–chloroform extraction and ethanol precipitation and transcribed into mRNAs for the next round of selection. From the second round of selection, the translation was performed at 5 µL scale, and the library

was first reversed transcribed by M-MLV before the pre-clear and positive selection. Six times of pre-clear were performed to remove beads binders more efficiently. Our first selection attempt of the mRNA-macrocycle fusion library using our ordinary protocol produced too rapidly enriched binder species in only two rounds, but our control experiments without the translation step also showed an increase in the recovery rate (data not shown). This suggested that the oligonucleotides (mRNA/cDNA) could interact non-specifically with the fibrils, disrupting the enrichment of our desired species of active macrocycle binders. Therefore, we modified the protocol of the RaPID selection by applying an excess amount of commercial yeast tRNAs to the selection process, with the aim of saturating the region(s) of the αSyn fibrils that could potentially interact with oligonucleotides. Finally, the observed enrichments at the seventh round were subjected to further DNA deep sequencing using the MiSeq sequencing system (Illumina). All DNA oligos were purchased from eurofins Genomics and are listed in Table S1.

Chemical Synthesis Of Peptides

Macrocyclic peptides were synthesized by standard Fmoc solid-phase peptide synthesis (SPPS) using a Syro Wave automated peptide synthesizer (Biotage). The resulting peptide–resin (25 μmol scale) was treated with a solution of 92.5% trifluoroacetic acid (TFA), 2.5% water, 2.5% triisopropylsilane and 2.5% ethanedithiol, to yield the free linear *N*-ClAc-peptide. Following diethyl ether precipitation, the pellet was dissolved in 10 ml triethylamine containing DMSO and incubated for 1 h at 25°C, to yield the corresponding macrocycle. The peptide suspensions were then acidified by addition of TFA to quench the macrocyclization reaction. The macrocycle was purified by RP-HPLC, using a Prominence HPLC system (Shimadzu) under linear gradient conditions. Mobile phase A (comprising water with 0.1% TFA) was mixed with mobile phase B (0.1% TFA in acetonitrile). Purified peptides were lyophilized *in vacuo* and molecular mass was confirmed by MALDI MS, using an Autoflex II instrument (Bruker Daltonics).

For the MTSL and fluorescein labelling of peptide-Cys, *N*-ClAc-peptide-Cys(Dpm)-NH-resin was synthesized by Fmoc SPPS. The Mmt group on Cys in the peptide sequence was then deprotected using a mixture of 98% dichloromethane, 3% TFA, and 2.5% triisopropylsilane. The resulting *N*-ClAc-peptide-Cys(Dpm)-NH-resin was cyclized by incubating overnight with 5% *N*,*N*-diisopropylethylamine (DIPEA) in *N*-methylpyrrolidone (NMP) at room temperature. The cleavage and purification of peptide-Cys-NH_2 were performed as described above. The obtained peptides were treated with the same equivalent of (1-Oxyl-2,2,5,5-tetramethyl-Δ3-pyrroline-3-methyl) methanethiosulfonate (MTSL, Toronto Research Chemicals Inc), fluorescein isothiocyanate (FITC, invitrogen), or Alexa568-maleimide (invitrogen) in DMSO. The resulting peptides were purified by RP-HPLC and lyophilized *in vacuo*. For the fluorescein labelling of peptide-$^{\beta}$Ala-Lys, Fmoc-peptide-Cys(Mmt)-NH-resin, which has Cys(Dpm) for cyclization and Cys(StBu) for free Cys in the peptide sequence, was synthesized by Fmoc SPPS. The Mmt group on Cys in peptide sequence was then deprotected using 98% dichloromethane, 3% TFA and 2.5% triisopropylsilane. The resulting Fmoc-peptide-Cys-NH-resin was treated with 4 equivalents of FITC in 5% DIPEA/NMP for 1 hour at room temperature. The Fmoc group on *N*-terminus of the peptide was deprotected using 20% piperidine and then chloroacetylated using ClAc-NHS. The cleavage and purification of *N*-ClAc-peptide-Cys(Fluor)-

NH_2 were performed as described above. The obtained *N*-ClAc-peptide-Cys(Fluor)-NH_2 was cyclized by incubating overnight with 5% DIPEA in NMP at room temperature. The StBu group on Cys in the peptide sequence was then deprotected using tributylphosphine with 10% H_2O, and the resulting peptides were purified by RP-HPLC and lyophilized *in vacuo*. Theoretical scores of water solubility of linear peptides were determined using the CamSol method[81].

Molecular cloning

pMGdB_sfGFP: The linear dsDNA encoding sfGFP gene was purchased from Integrated DNA Technologies. The pMGdB vector[82] was digested by XbaI (R0145, New England BioLabs) and XhoI (R0146, New England BioLabs). The gene was cloned into the linear vector by In-Fusion HD Cloning Kit (639648, Takara), yielding pMGdB_sfGFP.

pAC-Ptet_$FL2_{Linear}$-sfGFP: The DNA fragment encoding $FL2_{Linear}$ was prepared by assembly PCR using primers oligo1, oligo2 and oligo3. The linear vector encoding sfGFP was amplified by inverse PCR from pMGdB_sfGFP using prepared by oligo4 and oligo5. The gene was cloned into the linear vector by In-Fusion HD Cloning Kit, yielding pMGdB_$FL2_{Linear}$-sfGFP. The gene encoding $FL2_{Linear}$-sfGFP was amplified by PCR using primers oligo6 and oligo7. The linearized pAcTet vector was amplified by inverse PCR from pAC-Ptet-cpAaLS(119-aMD4L)[83] using oligo8 and oligo9. The gene was cloned into the linear vector by In-Fusion HD Cloning Kit, yielding pAC-Ptet_$FL2_{Linear}$-sfGFP.

pMGdB_$FD1_{Linear}$-sfGFP: The DNA fragment encoding $FD1_{Linear}$ was prepared by assembly PCR using primers oligo10, oligo11 and oligo12. The linear vector encoding sfGFP was amplified by inverse PCR from pMGdB_sfGFP using prepared by oligo13 and oligo14. The gene was cloned into the linear vector by In-Fusion HD Cloning Kit, yielding pMGdB_$FD1_{Linear}$-sfGFP.

All PCR products were purified by NucleoSpin Gel and PCR Clean-up (U0609A, MACHEREY-NAGEL). *Escherichia. coli* strain XL1-blue (200249, Agilent Technologies) was used as the host for plasmid preparation. All plasmids were purified using FastGene Plasmid Mini Kit (FG-90502, NIPPON Genetics). Plasmid sequences were confirmed by Sanger sequencing (FASMAC). All DNA oligos were purchased from eurofins Genomics and are listed in Table S1.

Protein expression and purification of $FL2_{Linear}$-sfGFP and $FD1_{Linear}$-sfGFP

E. coli BL21-gold (DE3)-pLysS competent cells (230134, Agilent Technologies) were transformed with pMGdB_sfGFP or pMGdB_$FD1_{Linear}$-sfGFP. The cells were grown at 37°C in Luria Bertani (LB) medium containing ampicillin (50 μg/mL) until the OD600 reached 0.4–0.6, at which point protein production was induced by adding isopropyl β-d-1-thiogalactopyranoside (IPTG) to a final concentration of 0.25 mM. Then, the cells were cultured at 20°C for 16 h. *E. coli* DH10B competent cells (EC0113, ThermoFischer) were transformed with pAC-Ptet_$FL2_{Linear}$-sfGFP. The cells were grown at 37°C in Luria Bertani (LB)

medium containing chloramphenicol (30 µg/mL) until the OD600 reached 0.4–0.6, at which point protein production was induced by adding tetracycline to a final concentration of 1 µg/mL. Then, the cells were cultured at 20°C for 16 h. Cells were harvested by centrifugation at 5,000 × *g* and 4°C for 10 min. Cells were resuspended in 15 mL lysis buffer [50 mM sodium phosphate buffer (pH 7.4), 1 M NaCl and 20 mM imidazole] After lysis by sonication and clearance by centrifugation at 15,000 × *g* and 25°C for 25 min, the supernatant was loaded onto 2 mL of Ni Separose 6 Fast Flow resin (Cytiva) in a gravity flow column. Beads were washed with lysis buffer, and protein was eluted with elution buffer [50 mM sodium phosphate buffer (pH 7.4), 200 mM NaCl and 500 mM imidazole]. The buffer was exchanged to PBS, using SnakeSkin Dialysis Tubing, 3.5K MWCO (ThermoFischer).

Isothermal Titration Calorimetry (Itc)

ITC measurements were performed to study the binding between αSyn fibrils and synthesized seven peptides using a Nano ITC instrument (TA Instruments). The peptides were dissolved in DMSO and a 100 mM peptide stock solution was prepared. A 1 mM peptide in PBS buffer (1% DMSO) was then injected into the sample cell containing approximately 190 µl of ultrasonicated αSyn fibrils (7th generation) at 100 µM in PBS with 1% DMSO. ITC titrations were carried out at 25°C with 2.5 µl injections for a total of 18 injections with stirring at 400 rpm. The data were fitted using an independent one-binding site model.

Phase Separation Assay

Solutions of monomeric αSyn were prepared by dissolving the lyophilized αSyn in 10 mM NaOH solution to achieve a neutral pH. The solutions were then filtered using a 0.22 µm filter, and the αSyn concentration was determined by NanoDrop. The resulting monomer was diluted with water to a concentration of 400 µM and stored at -80°C. Phase separation was induced by mixing αSyn dissolved in the desired buffer (pH7.5) with 10% PEG and the peptide dissolved in 100% DMSO at a concentration of 100 µM. The peptide solution was then diluted to be a final concentration of 1% DMSO. Differential Interference Contrast (DIC) images were obtained at room temperature using a Leica DMI6000 B microscope with a 40× objective lens. All the images were obtained at resolution of 696×520 pixels at 24-bit depth. The αSyn concentration was fixed at 100 µM unless otherwise stated. For turbidimetry, 100 µM of αSyn in the presence of 10% PEG was incubated for 30 min at 4°C with various concentrations of peptides before measurements. The measurements were carried out using a spectrometer Jasco V670 (JASCO) with excitation and emission at 600 nm. Temperature regulation was carried out using a Peltier-unit (JASCO) with a 1 mm light path cell.

For confocal microscopy, we used mixture of 1% FL2C-Fluor or FD1C-Fluor and 99% non-labeled FL2 or FD1 as LLPS inducer peptides for αSyn (Fig. 2f, g). Non-labelled wild-type α-synuclein was mixed with αSyn-Rhod at a 99:1 molar ratio. αSyn formed aggregate-like assemblies with 100% FD1C-Fluor due to its low solubility, whereas αSyn formed spherical droplets with 100% FD1-sfGFP (**Supplementary Fig. 6b, c**). To minimize the effect of FL2C-Fluor and FD1C-Fluor on the liquidity of formed αSyn droplets, we decided

to use low concentration of FL2C-Fluor and FD1C-Fluor by mixing them with non-labeled FL2 and FD1 for confocal microscopy. Fluorescein and sfGFP without peptide-tag did not show efficient localization in αSyn droplets induced by FL2 and FD1 (**Supplementary Fig. 6d, e**).

Confocal Microscopy

The fusion event of αSyn liquid droplets in vitro was visualized with a using a Leica TCS SP8 confocal microscope with a 63× oil objective lens at room temperature. Rhodamine-labeled αSyn, fluorescein-labeled peptide, peptide-tagged sfGFP, Thiolfavin T (ThT) (Wako Pure Chemical Industries Ltd.), and 1-anilinonaphthalene-8-sulfonic acid (ANS) (Nacalai Tesque) were observed using appropriate fluorescence channels (488 nm for fluorescein and sfGFP, 561 nm for rhodamine,, 442 nm for ThT, and 405 nm for ANS). All the images were captured at a resolution of 512×512 pixels at 24-bit depth. Fluorescence Recovery After Photobleaching (FRAP) measurements were performed using a Leica TCS SP8 confocal microscope. A region of interest (ROI) with a radius of 1.0 μm was bleached using an appropriate laser, and the recovery of the bleached spots was recorded using the software provided with the instrument. The fluorescence recovery was background-corrected, normalized, and plotted using Igor Pro.

Nmr Measurements

^{15}N-αSyn was dissolved in 20 mM sodium phosphate buffer (pH 7.4), 2% (v/v) D_2O, and 100 mM FL2 and FD1, which were dissolved in DMSO, were diluted to 100 μM and 200 μM, respectively (0.1% DMSO in final solution). Different concentration of FL2 and FD1 were used based on their LLPS efficiency, and the pH of the mixture was checked immediately before measurement. The spectra were measured at 4°C using a Bruker Avance-III 950 MHz spectrometer equipped with a cryogenic probe, and 16 scans were taken for each spectrum. Signal assignments were achieved by comparing the chemical shifts to those previously published[84] and obtained from the temperature- and PEG-concentration-titration measurements. Chemical shift perturbations (CSP) were calculated as $\Delta\delta = ((\Delta\delta_N/5)^2 + (\Delta\delta_{HN})^2)^{1/2}$. For PRE measurements, nitroxide spin-labeled FD1 (FD1-C21R1) was synthesized as described in the synthesis section, and 10 molar equivalent of 10% FD1-C21R1 ([FD1]:[FD1-C21R1] = 9:1) were added to a 100 μM ^{15}N-αSyn solution. The NMR spectra were processed using TopSpin 4.0 (Bruker), and resonance assignment and intensity calculations were performed using the Sparky Program.

Fluorescence Assay

The αSyn monomer was diluted to the desired concentration with a 10×PBS buffer and supplemented with 20 μM ThT and 50 μM ANS from a 1 mM stock. All samples were prepared in low-binding Eppendorf tubes on ice. Each sample was then pipetted into multiple wells of a 96-well half-area, low-binding polyethylene glycol coating plate (Corning 3881) with a clear bottom, at 80 μl per well. Assays were initiated by placing the 96-well plate at 37°C with a cycle of 3 min shaking and 27 min quiescence in a

plate reader (Flex station; Molecular Devices). The fluorescence of ThT and ANS was measured through the bottom of the plate with a 440 nm and 380 nm excitation filter, respectively, and a 480 nm emission filter, with three repeats per sample.

Declarations

We declare no competing interests with regards to this submission.

Acknowledgements

This work was supported by JST, ACT-X Grant Number JP21456855, Japan to T.I. and a Technology Licensing Fund to H.S.. NMR studies were performed in part using the NMR spectrometers with the ultra-high magnetic fields under the Collaborative Research Program of Institute for protein research, Osaka University, NMRCR-21-05.

Author Contributions

T.I. and H.S. were involved in the design of research. T.I. performed all in vitro experiments. M.S. and Y.G. contributed to NMR measurements. Y.K. provided $\alpha Syn_{1\text{-}103}$, $\alpha Syn_{104\text{-}140,}$ and plasmid of αSyn. N.T. and W.E.H. prepared peptide-tagged proteins. T.I and H.S. wrote the paper. All authors discussed the results and commented on the manuscript.

References

1. Shin, Y. & Brangwynne, C. P. Liquid phase condensation in cell physiology and disease. Science 357, doi:10.1126/science.aaf4382 (2017).
2. Alberti, S., Gladfelter, A. & Mittag, T. Considerations and Challenges in Studying Liquid-Liquid Phase Separation and Biomolecular Condensates. Cell 176, 419–434, doi:10.1016/j.cell.2018.12.035 (2019).
3. Banani, S. F., Lee, H. O., Hyman, A. A. & Rosen, M. K. Biomolecular condensates: organizers of cellular biochemistry. Nat Rev Mol Cell Biol 18, 285–298, doi:10.1038/nrm.2017.7 (2017).
4. Patel, A. *et al.* A Liquid-to-Solid Phase Transition of the ALS Protein FUS Accelerated by Disease Mutation. Cell 162, 1066–1077, doi:10.1016/j.cell.2015.07.047 (2015).
5. Ambadipudi, S., Biernat, J., Riedel, D., Mandelkow, E. & Zweckstetter, M. Liquid-liquid phase separation of the microtubule-binding repeats of the Alzheimer-related protein Tau. Nat Commun 8, 275, doi:10.1038/s41467-017-00480-0 (2017).
6. Kanaan, N. M., Hamel, C., Grabinski, T. & Combs, B. Liquid-liquid phase separation induces pathogenic tau conformations in vitro. Nat Commun 11, 2809, doi:10.1038/s41467-020-16580-3 (2020).
7. Mathieu, C., Pappu, R. V. & Taylor, J. P. Beyond aggregation: Pathological phase transitions in neurodegenerative disease. Science 370, 56–60, doi:10.1126/science.abb8032 (2020).

8. Aguzzi, A. & Altmeyer, M. Phase Separation: Linking Cellular Compartmentalization to Disease. Trends Cell Biol 26, 547–558, doi:10.1016/j.tcb.2016.03.004 (2016).
9. Molliex, A. *et al.* Phase separation by low complexity domains promotes stress granule assembly and drives pathological fibrillization. Cell 163, 123–133, doi:10.1016/j.cell.2015.09.015 (2015).
10. Brangwynne, C. P., Tompa, P. & Pappu, R. V. Polymer physics of intracellular phase transitions. Nat Phys 11, 899–904, doi:10.1038/Nphys3532 (2015).
11. Boeynaems, S. *et al.* Protein Phase Separation: A New Phase in Cell Biology. Trends Cell Biol 28, 420–435, doi:10.1016/j.tcb.2018.02.004 (2018).
12. Li, P. *et al.* Phase transitions in the assembly of multivalent signalling proteins. Nature 483, 336–340, doi:10.1038/nature10879 (2012).
13. Yuan, C. *et al.* Nucleation and Growth of Amino Acid and Peptide Supramolecular Polymers through Liquid-Liquid Phase Separation. Angew Chem Int Ed Engl 58, 18116–18123, doi:10.1002/anie.201911782 (2019).
14. Levin, A. *et al.* Ostwald's rule of stages governs structural transitions and morphology of dipeptide supramolecular polymers. Nat Commun 5, 5219, doi:10.1038/ncomms6219 (2014).
15. Bracha, D. *et al.* Mapping Local and Global Liquid Phase Behavior in Living Cells Using Photo-Oligomerizable Seeds. *Cell* 175, 1467–1480 e1413, doi:10.1016/j.cell.2018.10.048 (2018).
16. Reinkemeier, C. D., Girona, G. E. & Lemke, E. A. Designer membraneless organelles enable codon reassignment of selected mRNAs in eukaryotes. Science 363, doi:10.1126/science.aaw2644 (2019).
17. Heidenreich, M. *et al.* Designer protein assemblies with tunable phase diagrams in living cells. Nat Chem Biol 16, 939–945, doi:10.1038/s41589-020-0576-z (2020).
18. Dzuricky, M., Rogers, B. A., Shahid, A., Cremer, P. S. & Chilkoti, A. De novo engineering of intracellular condensates using artificial disordered proteins. Nat Chem 12, 814–825, doi:10.1038/s41557-020-0511-7 (2020).
19. Santofimia-Castano, P. *et al.* Targeting intrinsically disordered proteins involved in cancer. Cell Mol Life Sci 77, 1695–1707, doi:10.1007/s00018-019-03347-3 (2020).
20. Ruan, H., Sun, Q., Zhang, W., Liu, Y. & Lai, L. Targeting intrinsically disordered proteins at the edge of chaos. Drug Discov Today 24, 217–227, doi:10.1016/j.drudis.2018.09.017 (2019).
21. Chiti, F. & Dobson, C. M. Protein misfolding, functional amyloid, and human disease. Annu Rev Biochem 75, 333–366, doi:10.1146/annurev.biochem.75.101304.123901 (2006).
22. Dawson, T. M. & Dawson, V. L. Molecular pathways of neurodegeneration in Parkinson's disease. Science 302, 819–822, doi:10.1126/science.1087753 (2003).
23. Dettmer, U., Selkoe, D. & Bartels, T. New insights into cellular alpha-synuclein homeostasis in health and disease. Curr Opin Neurobiol 36, 15–22, doi:10.1016/j.conb.2015.07.007 (2016).
24. Knowles, T. P., Vendruscolo, M. & Dobson, C. M. The amyloid state and its association with protein misfolding diseases. Nat Rev Mol Cell Biol 15, 384–396, doi:10.1038/nrm3810 (2014).

25. Spillantini, M. G., Crowther, R. A., Jakes, R., Hasegawa, M. & Goedert, M. alpha-Synuclein in filamentous inclusions of Lewy bodies from Parkinson's disease and dementia with lewy bodies. Proc Natl Acad Sci U S A 95, 6469–6473, doi:10.1073/pnas.95.11.6469 (1998).
26. Ray, S. *et al.* alpha-Synuclein aggregation nucleates through liquid-liquid phase separation. Nat Chem 12, 705–716, doi:10.1038/s41557-020-0465-9 (2020).
27. Sawner, A. S. *et al.* Modulating alpha-Synuclein Liquid-Liquid Phase Separation. Biochemistry 60, 3676–3696, doi:10.1021/acs.biochem.1c00434 (2021).
28. Heller, G. T., Sormanni, P. & Vendruscolo, M. Targeting disordered proteins with small molecules using entropy. Trends Biochem Sci 40, 491–496, doi:10.1016/j.tibs.2015.07.004 (2015).
29. Heller, G. T., Bonomi, M. & Vendruscolo, M. Structural Ensemble Modulation upon Small-Molecule Binding to Disordered Proteins. J Mol Biol 430, 2288–2292, doi:10.1016/j.jmb.2018.03.015 (2018).
30. Heller, G. T. *et al.* Small-molecule sequestration of amyloid-beta as a drug discovery strategy for Alzheimer's disease. Sci Adv 6, doi:10.1126/sciadv.abb5924 (2020).
31. Tuttle, M. D. *et al.* Solid-state NMR structure of a pathogenic fibril of full-length human alpha-synuclein. Nat Struct Mol Biol 23, 409–415, doi:10.1038/nsmb.3194 (2016).
32. Li, B. *et al.* Cryo-EM of full-length alpha-synuclein reveals fibril polymorphs with a common structural kernel. Nat Commun 9, 3609, doi:10.1038/s41467-018-05971-2 (2018).
33. Guerrero-Ferreira, R. *et al.* Cryo-EM structure of alpha-synuclein fibrils. Elife 7, doi:10.7554/eLife.36402 (2018).
34. Ito, K., Passioura, T. & Suga, H. Technologies for the synthesis of mRNA-encoding libraries and discovery of bioactive natural product-inspired non-traditional macrocyclic peptides. Molecules 18, 3502–3528, doi:10.3390/molecules18033502 (2013).
35. Josephson, K., Ricardo, A. & Szostak, J. W. mRNA display: from basic principles to macrocycle drug discovery. Drug Discov Today 19, 388–399, doi:10.1016/j.drudis.2013.10.011 (2014).
36. Goto, Y., Katoh, T. & Suga, H. Flexizymes for genetic code reprogramming. Nat Protoc 6, 779–790, doi:10.1038/nprot.2011.331 (2011).
37. Chen, S., Bertoldo, D., Angelini, A., Pojer, F. & Heinis, C. Peptide ligands stabilized by small molecules. Angew Chem Int Ed Engl 53, 1602–1606, doi:10.1002/anie.201309459 (2014).
38. Angelini, A. *et al.* Bicyclic peptide inhibitor reveals large contact interface with a protease target. ACS Chem Biol 7, 817–821, doi:10.1021/cb200478t (2012).
39. Bionda, N. & Fasan, R. Ribosomal Synthesis of Natural-Product-Like Bicyclic Peptides in Escherichia coli. Chembiochem 16, 2011–2016, doi:10.1002/cbic.201500179 (2015).
40. Fitzpatrick, A. W. P. *et al.* Cryo-EM structures of tau filaments from Alzheimer's disease. Nature 547, 185–190, doi:10.1038/nature23002 (2017).
41. Agarwal, A., Arora, L., Rai, S. K., Avni, A. & Mukhopadhyay, S. Spatiotemporal modulations in heterotypic condensates of prion and alpha-synuclein control phase transitions and amyloid conversion. Nat Commun 13, 1154, doi:10.1038/s41467-022-28797-5 (2022).

42. Shakya, A. & King, J. T. DNA Local-Flexibility-Dependent Assembly of Phase-Separated Liquid Droplets. Biophys J 115, 1840–1847, doi:10.1016/j.bpj.2018.09.022 (2018).
43. Ura, T., Tomita, S. & Shiraki, K. Dynamic behavior of liquid droplets with enzyme compartmentalization triggered by sequential glycolytic enzyme reactions. Chem Commun (Camb) 57, 12544–12547, doi:10.1039/d1cc04596b (2021).
44. Nakashima, K. K., Baaij, J. F. & Spruijt, E. Reversible generation of coacervate droplets in an enzymatic network. Soft Matter 14, 361–367, doi:10.1039/c7sm01897e (2018).
45. Koga, S., Williams, D. S., Perriman, A. W. & Mann, S. Peptide-nucleotide microdroplets as a step towards a membrane-free protocell model. Nat Chem 3, 720–724, doi:10.1038/nchem.1110 (2011).
46. Fisher, R. S. & Elbaum-Garfinkle, S. Tunable multiphase dynamics of arginine and lysine liquid condensates. Nat Commun 11, 4628, doi:10.1038/s41467-020-18224-y (2020).
47. Doherty, C. P. A. *et al.* A short motif in the N-terminal region of alpha-synuclein is critical for both aggregation and function. Nat Struct Mol Biol 27, 249–259, doi:10.1038/s41594-020-0384-x (2020).
48. Portz, B., Lee, B. L. & Shorter, J. FUS and TDP-43 Phases in Health and Disease. Trends Biochem Sci 46, 550–563, doi:10.1016/j.tibs.2020.12.005 (2021).
49. Tange, H. *et al.* Liquid-liquid phase separation of full-length prion protein initiates conformational conversion in vitro. J Biol Chem 296, 100367, doi:10.1016/j.jbc.2021.100367 (2021).
50. Ishizawa, T., Mattila, P., Davies, P., Wang, D. & Dickson, D. W. Colocalization of tau and alpha-synuclein epitopes in Lewy bodies. J Neuropathol Exp Neurol 62, 389–397, doi:10.1093/jnen/62.4.389 (2003).
51. Uchikado, H., Lin, W. L., DeLucia, M. W. & Dickson, D. W. Alzheimer disease with amygdala Lewy bodies: a distinct form of alpha-synucleinopathy. J Neuropathol Exp Neurol 65, 685–697, doi:10.1097/01.jnen.0000225908.90052.07 (2006).
52. Kovacs, G. G. *et al.* The prion protein in human neurodegenerative disorders. Neurosci Lett 329, 269–272, doi:10.1016/s0304-3940(02)00668-7 (2002).
53. Biancalana, M. & Koide, S. Molecular mechanism of Thioflavin-T binding to amyloid fibrils. Biochim Biophys Acta 1804, 1405–1412, doi:10.1016/j.bbapap.2010.04.001 (2010).
54. Vassar, P. S. & Culling, C. F. Fluorescent stains, with special reference to amyloid and connective tissues. Arch Pathol 68, 487–498 (1959).
55. Ma, L., Fang, X. & Wang, C. Peptide-based coacervates in therapeutic applications. Front Bioeng Biotechnol 10, 1100365, doi:10.3389/fbioe.2022.1100365 (2022).
56. Babu, M. M., van der Lee, R., de Groot, N. S. & Gsponer, J. Intrinsically disordered proteins: regulation and disease. Curr Opin Struct Biol 21, 432–440, doi:10.1016/j.sbi.2011.03.011 (2011).
57. Tompa, P. Intrinsically disordered proteins: a 10-year recap. Trends Biochem Sci 37, 509–516, doi:10.1016/j.tibs.2012.08.004 (2012).
58. Metallo, S. J. Intrinsically disordered proteins are potential drug targets. Curr Opin Chem Biol 14, 481–488, doi:10.1016/j.cbpa.2010.06.169 (2010).

59. Uversky, V. N., Oldfield, C. J. & Dunker, A. K. Intrinsically disordered proteins in human diseases: introducing the D2 concept. Annu Rev Biophys 37, 215–246, doi:10.1146/annurev.biophys.37.032807.125924 (2008).
60. Russ, A. P. & Lampel, S. The druggable genome: an update. Drug Discov Today 10, 1607–1610, doi:10.1016/S1359-6446(05)03666-4 (2005).
61. Hopkins, A. L. & Groom, C. R. The druggable genome. Nat Rev Drug Discov 1, 727–730, doi:10.1038/nrd892 (2002).
62. Klein, I. A. *et al.* Partitioning of cancer therapeutics in nuclear condensates. Science 368, 1386–1392, doi:10.1126/science.aaz4427 (2020).
63. O'Flynn, B. G. & Mittag, T. The role of liquid-liquid phase separation in regulating enzyme activity. Curr Opin Cell Biol 69, 70–79, doi:10.1016/j.ceb.2020.12.012 (2021).
64. Rogers, J. M., Passioura, T. & Suga, H. Nonproteinogenic deep mutational scanning of linear and cyclic peptides. Proc Natl Acad Sci U S A 115, 10959–10964, doi:10.1073/pnas.1809901115 (2018).
65. Hardenberg, M., Horvath, A., Ambrus, V., Fuxreiter, M. & Vendruscolo, M. Widespread occurrence of the droplet state of proteins in the human proteome. Proc Natl Acad Sci U S A 117, 33254–33262, doi:10.1073/pnas.2007670117 (2020).
66. Stephens, A. D. *et al.* Extent of N-terminus exposure of monomeric alpha-synuclein determines its aggregation propensity. Nat Commun 11, 2820, doi:10.1038/s41467-020-16564-3 (2020).
67. Theillet, F. X. *et al.* Structural disorder of monomeric alpha-synuclein persists in mammalian cells. Nature 530, 45–50, doi:10.1038/nature16531 (2016).
68. Bertoncini, C. W. *et al.* Release of long-range tertiary interactions potentiates aggregation of natively unstructured alpha-synuclein. Proc Natl Acad Sci U S A 102, 1430–1435, doi:10.1073/pnas.0407146102 (2005).
69. Tartaglia, G. G. & Vendruscolo, M. The Zyggregator method for predicting protein aggregation propensities. Chem Soc Rev 37, 1395–1401, doi:10.1039/b706784b (2008).
70. You, K. *et al.* PhaSepDB: a database of liquid-liquid phase separation related proteins. Nucleic Acids Res 48, D354-D359, doi:10.1093/nar/gkz847 (2020).
71. Meszaros, B. *et al.* PhaSePro: the database of proteins driving liquid-liquid phase separation. Nucleic Acids Res 48, D360-D367, doi:10.1093/nar/gkz848 (2020).
72. Wang, X. *et al.* LLPSDB v2.0: an updated database of proteins undergoing liquid-liquid phase separation in vitro. Bioinformatics, doi:10.1093/bioinformatics/btac026 (2022).
73. Li, Q. *et al.* LLPSDB: a database of proteins undergoing liquid-liquid phase separation in vitro. Nucleic Acids Res 48, D320-D327, doi:10.1093/nar/gkz778 (2020).
74. Murray, D. T. *et al.* Structure of FUS Protein Fibrils and Its Relevance to Self-Assembly and Phase Separation of Low-Complexity Domains. *Cell* 171, 615–627 e616, doi:10.1016/j.cell.2017.08.048 (2017).

75. Dada, S. T. *et al.* Spontaneous nucleation and fast aggregate-dependent proliferation of alpha-synuclein aggregates within liquid condensates at neutral pH. Proc Natl Acad Sci U S A 120, e2208792120, doi:10.1073/pnas.2208792120 (2023).
76. So, M., Hall, D. & Goto, Y. Revisiting supersaturation as a factor determining amyloid fibrillation. Curr Opin Struct Biol 36, 32–39, doi:10.1016/j.sbi.2015.11.009 (2016).
77. Yagi, H., Kusaka, E., Hongo, K., Mizobata, T. & Kawata, Y. Amyloid fibril formation of alpha-synuclein is accelerated by preformed amyloid seeds of other proteins: implications for the mechanism of transmissible conformational diseases. J Biol Chem 280, 38609–38616, doi:10.1074/jbc.M508623200 (2005).
78. Tycko, R. Physical and structural basis for polymorphism in amyloid fibrils. Protein Sci 23, 1528–1539, doi:10.1002/pro.2544 (2014).
79. Hayashi, Y., Morimoto, J. & Suga, H. In vitro selection of anti-Akt2 thioether-macrocyclic peptides leading to isoform-selective inhibitors. ACS Chem Biol 7, 607–613, doi:10.1021/cb200388k (2012).
80. Ikenoue, T. *et al.* Cold denaturation of alpha-synuclein amyloid fibrils. Angew Chem Int Ed Engl 53, 7799–7804, doi:10.1002/anie.201403815 (2014).
81. Sormanni, P., Aprile, F. A. & Vendruscolo, M. The CamSol method of rational design of protein mutants with enhanced solubility. J Mol Biol 427, 478–490, doi:10.1016/j.jmb.2014.09.026 (2015).
82. Terasaka, N., Azuma, Y. & Hilvert, D. Laboratory evolution of virus-like nucleocapsids from nonviral protein cages. Proc Natl Acad Sci U S A 115, 5432–5437, doi:10.1073/pnas.1800527115 (2018).
83. Komatsu, Y. *et al.* De novo peptide grafting to a self-assembling nanocapsule yields a hepatocyte growth factor receptor agonist. iScience 24, 103302, doi:10.1016/j.isci.2021.103302 (2021).
84. Bermel, W. *et al.* Protonless NMR experiments for sequence-specific assignment of backbone nuclei in unfolded proteins. J Am Chem Soc 128, 3918–3919, doi:10.1021/ja0582206 (2006).

Figures

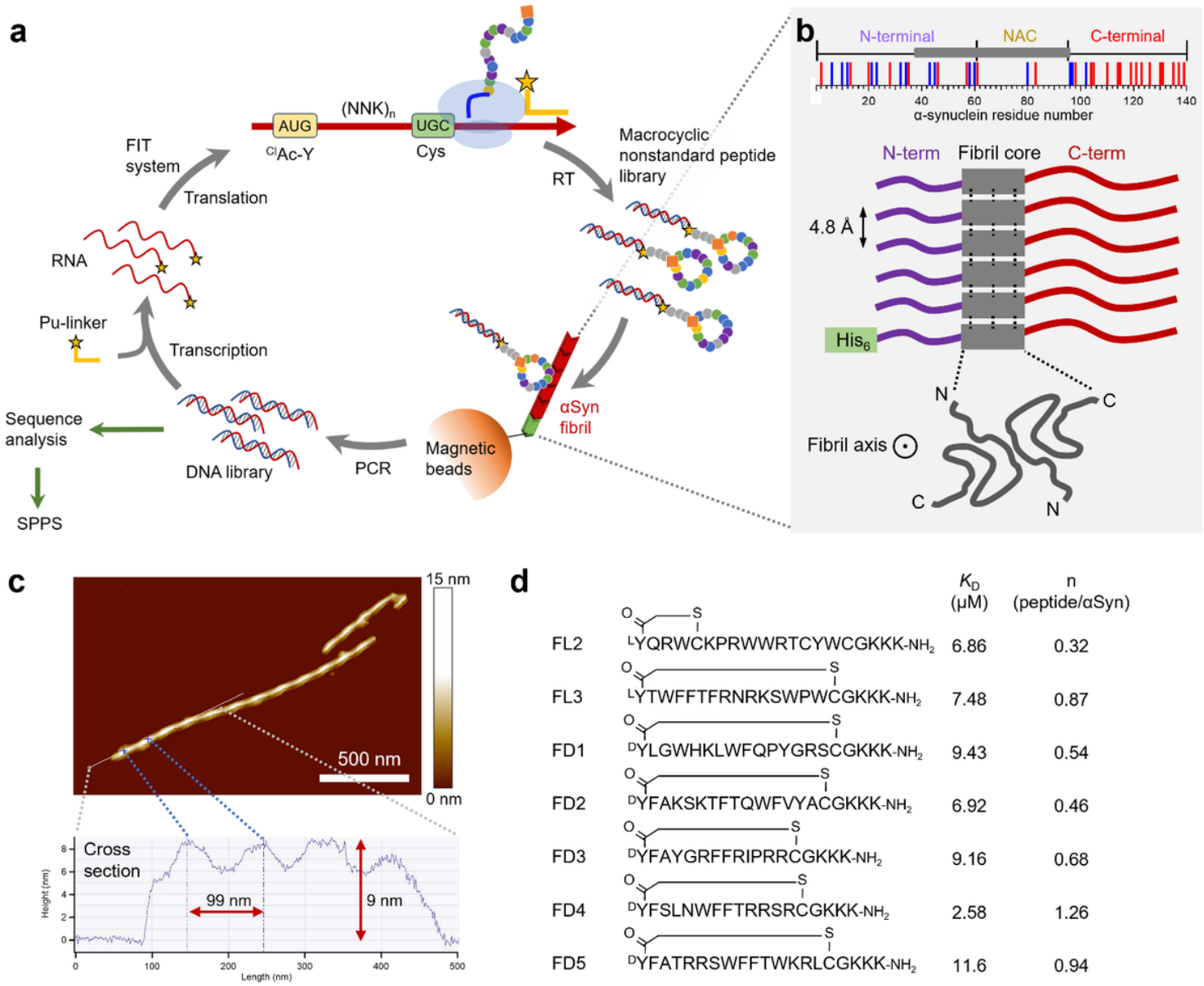

Figure 1

Selection of macrocyclic peptides that interact with the amyloid fibrils of αSyn

a Overview of the RaPID system for macrocyclic peptides. The messenger RNA library containing a random sequence domain, $(NNK)_{6\text{-}15}$, was transcribed from the corresponding cDNA library and were conjugated with an oligonucleotide bearing puromycin. The resulting mRNAs were translated by the FIT system in the presence of the appropriate aminoacyl-tRNAs prepared by flexizymes. Linear peptides displayed on the individual mRNAs were spontaneously cyclized after translation, and the resulting macrocyclic peptides were displayed. After reverse transcription, the peptide libraries were subjected to αSyn fibrils immobilized on magnetic beads, and binding species were isolated. The cDNAs on binding mRNA-peptide fusion were recovered and amplified by PCR. b The position of charged residues of the αSyn sequence (top) and a schematic depiction of the typical structure of amyloid fibrils of αSyn (bottom) are shown. The negatively and positively charged residues of the corresponding monomer at

neutral pH are shown by red and blue bars, respectively. The core region in the fibrils is signified by gray rectangles. The arrangement of the two protofilaments is illustrated as a cross-section of the fibril core[32]. c AFM image of a morphology of αSyn fibrils displayed during the peptide selection. The seeding of αSyn fibrils was repeated six times to uniform the morphology of fibrils. d Peptide sequences were identified from the pool in round six. The dissociation constant K_D and the molar binding ratio of the peptides to αSyn were elucidated by ITC.

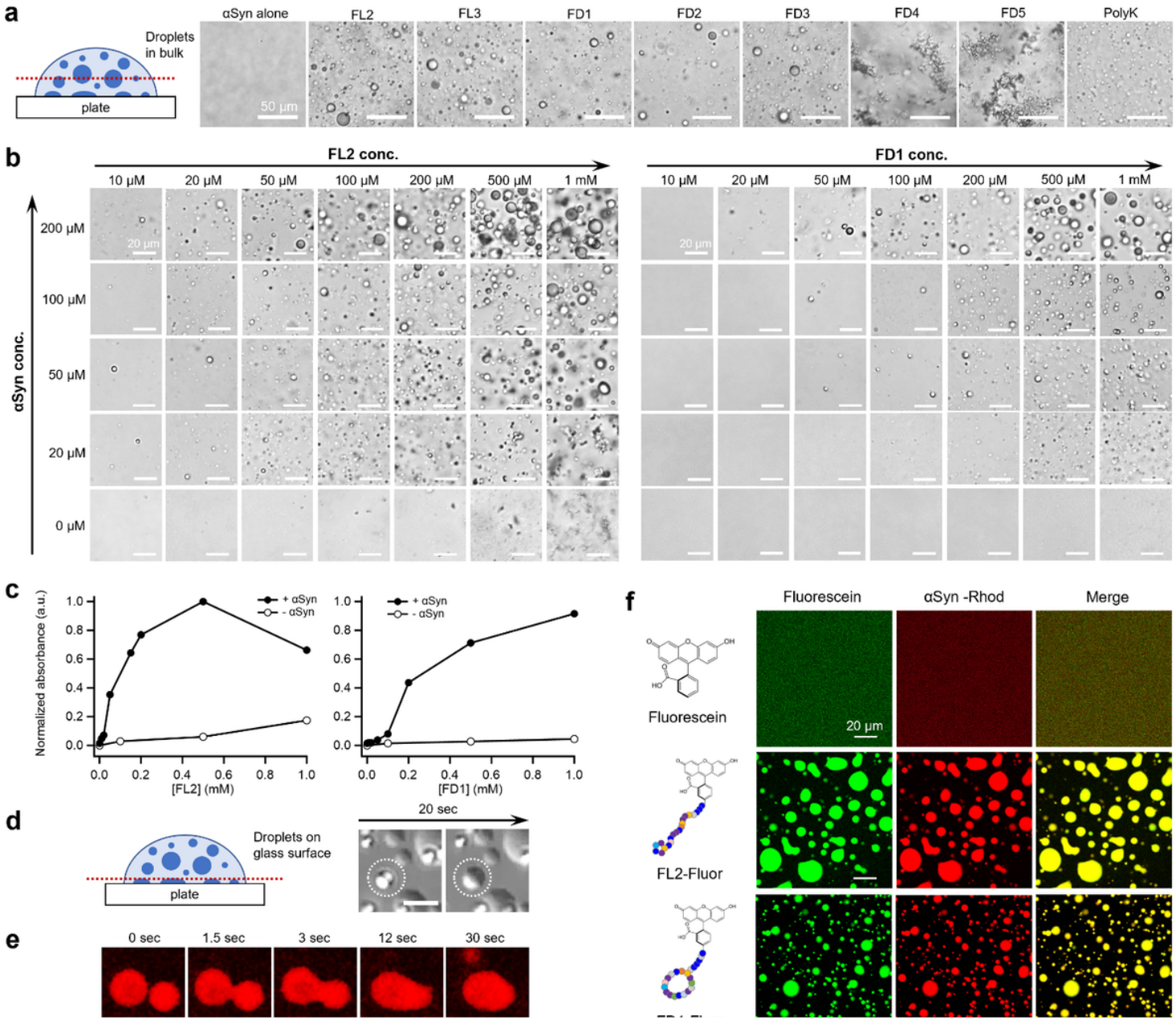

Figure 2

Selected peptides induce LLPS of αSyn and are co-localized with αSyn in liquid droplets.

aDIC images of the αSyn solution in the absence and presence of the selected 7 peptides and polyK after 1 h incubation on ice. All solutions were prepared with 20 mM NaPi at pH 7.5 and 10% PEG8000. b A series of DIC images of αSyn solution at various concentrations of FL2 (left) and FD1 (right) after 30 min incubation at 4 °C. The scale bar on the DIC images indicates 20 μm. c Turbidity at 600 nm was measured at various concentrations of FL2 and FD1 in the absence and presence of αSyn. d Adsorption of a droplet onto the glass surface observed by DIC. The scale bars indicate 10 μm. e Fusion event of two droplets on the glass surface observed by confocal microscopy with the rhodamine labeled αSyn (αSyn-Rhod). fFluorescence images of solutions containing αSyn-Rhodand Fluorescein-labeled FL2 (FL2C-Fluor) and FD1 (FD1C-Fluor) represent colocalization in the droplets.

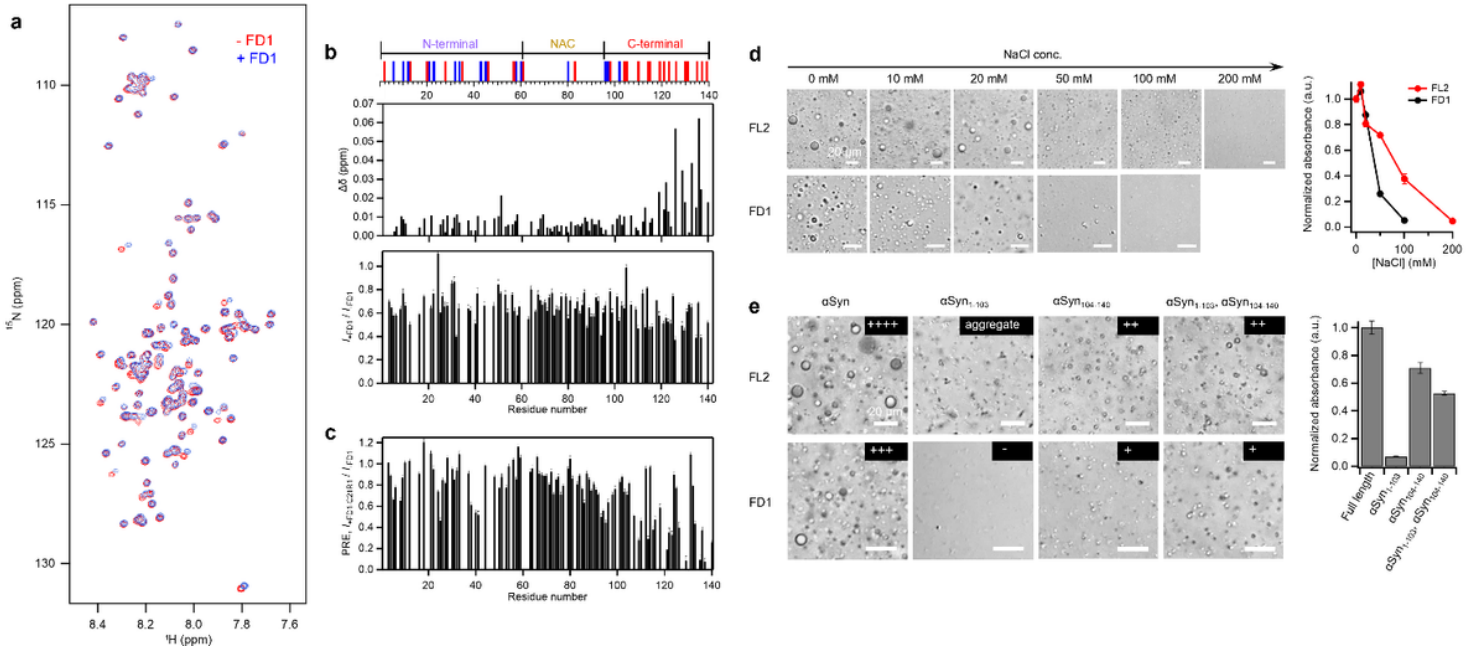

Figure 3

Peptides mainly interact with the C-terminal region of αSyn via electrostatic interactions

a ^{1}H-^{15}N-HSQC spectrum of 100 μM ^{15}N-labeled αSyn monomers in the absence (red) and presence (blue) of 200 μM FD1. b Chemical shift differences (Δδ) and peak intensity ratios (I_{+FD1}/I_{-FD1}) of αSyn in the presence of FD1 suggest interaction of FD1 with the C-terminal region of monomeric αSyn. c PRE-NMR normalized intensity ratio ($I_{+FD1\text{-}C21R1}/I_{-FD1}$) of αSyn generated using MTSL labeled FD1-C21R1 showed significant decrease at both N- and C-terminus of αSyn. d DIC images and turbidity at 600 nm show a salt concentration dependence of the formation of droplets in the presence of 100 μM of FL2 and FD1. e Comparison of LLPS efficiency of the full-length αSyn and the charge-deleted mutants ($αSyn_{1\text{-}103}$ and $αSyn_{104\text{-}140}$) with 400 μM of FL2 and FD1 observed by DIC images. Turbidity of solution with FD1 is shown on the right.

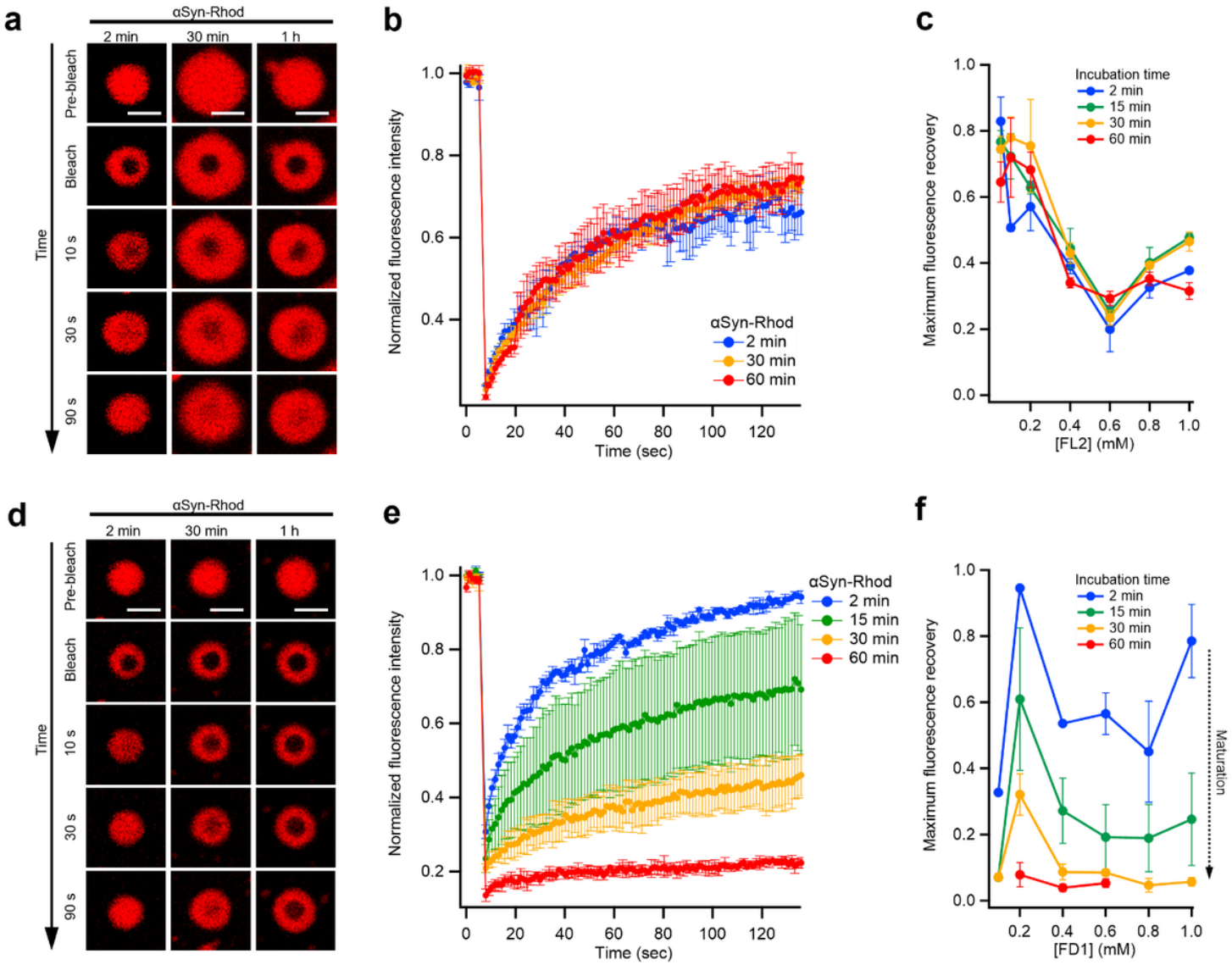

Figure 4

Fluidity of αSyn-Rhod in liquid droplets induced by FL2 and FD1

aRepresentative fluorescence images of αSyn-FL2 droplets during FRAP measurements at various incubation time points (2, 30, and 60 min) at room temperature. b FRAP kinetics for each incubation time point show high liquidity and low maturation propensity. c Comparison of maximum fluorescence recovery of αSyn-Rhodafter photobleaching (130 sec) at various FL2 concentrations (0.05, 0.1, 0.2, 0.4, 0.6, 0.8, and 1.0 mM) shows concentration-dependent liquidity and no time-dependent maturation at each FL2 concentration. d Representative fluorescence images of αSyn-FD1 droplets during FRAP measurements at various incubation time points (2, 15, 30, and 60 min) at room temperature. e FRAP kinetics for each incubation time point show that the liquid droplets lose their liquidity as time passes. f Comparison of maximum fluorescence recovery of αSyn-Rhodafter photobleaching (130 sec) at various FD1 concentrations (0.1, 0.2, 0.4, 0.6, 0.8, and 1.0 mM) shows a concentration-dependent liquidity and

high time-dependent maturation propensity at each FD1 concentration. The data represent the mean±STD for n=3 independent experiments.

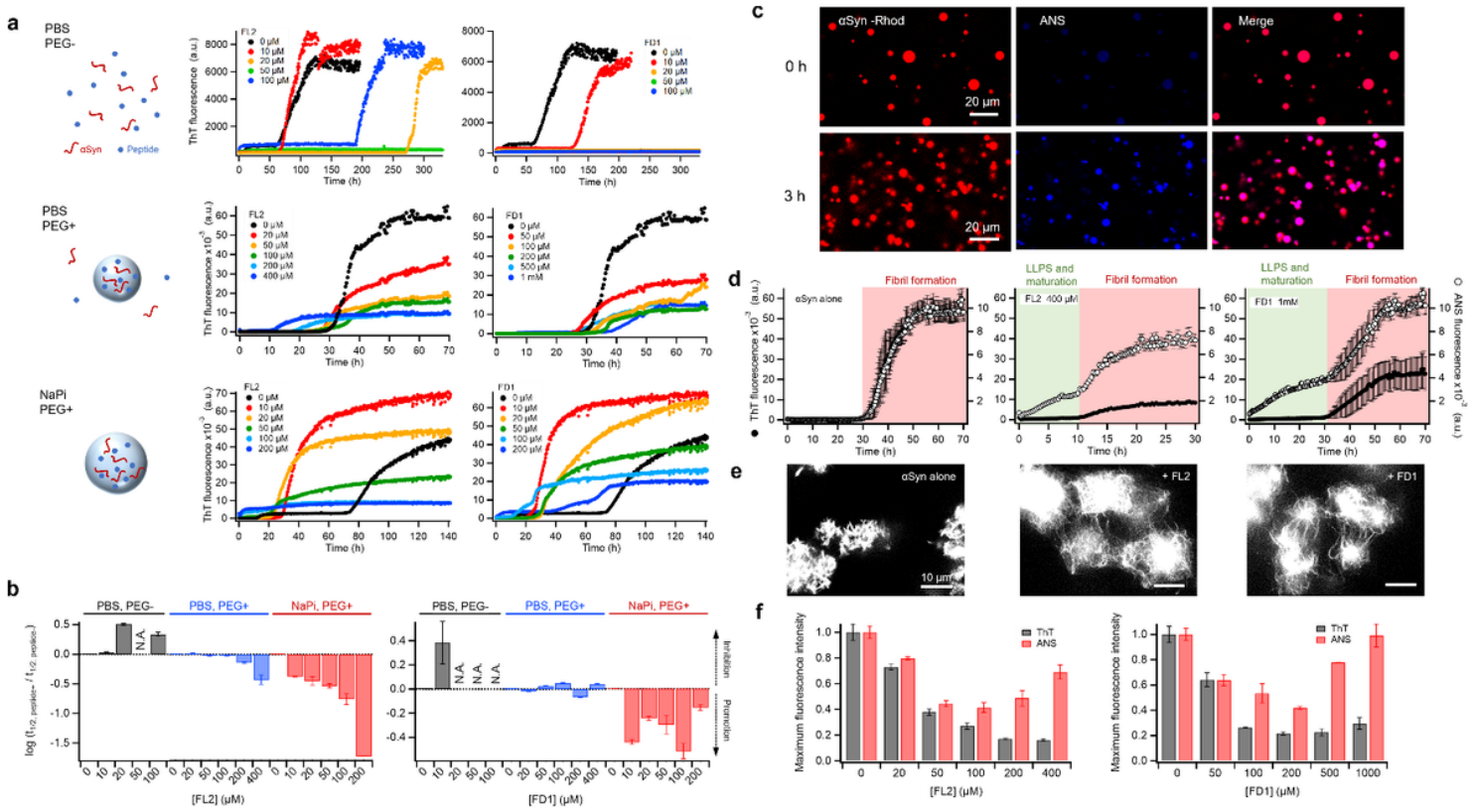

Figure 5

Aggregation of αSyn is accelerated under conditions promoting LLPS

a ThT kinetic profile of αSyn aggregation under different conditions, including αSyn is dissolved in PBS without PEG-8000 (upper), PBS with 10% PEG-8000 (middle), or NaPi with 10% PEG-8000 (lower), in the presence and absence of various concentrations of FL2 and FD1 (represented by different colors). b Comparison of the lag-time of the αSyn fibril formation in the presence of peptides to the one in the absence of the peptides ($log(t_{1/2,peptide+}/t_{1/2,\ peptide-})$) shows acceleration of aggregation under conditions promoting LLPS. Lag-times ofαSyn fibril formation in PBS without PEG-8000 at high peptide concentrations are not available because ThT increase was not observed within the 14-day time scale. c Fluorescence images of the droplets formed in the presence of 400 μM FL2 show an increase in ANS fluorescence intensity in the droplets after 3 h incubation at 37 °C. d Simultaneous observation of ThT (closed circle) and ANS (opened circle) fluorescence during the αSyn aggregation in PBS with 10% PEG-8000 reveals two-step fibril formation modalities, with an early LLPS and maturation phase (ANS increase colored by green area) and subsequent fibril formation (ThT increase colored by red area). e Fluorescence images show morphological changes of the aggregates after 70 h incubation in the presence of the peptides. f Comparison of maximum intensity of ThT (black) and ANS (red) at various peptide concentrations indicates that αSyn forms more ANS positive aggregates at high peptide concentrations, whereas the ThT intensity decreases.

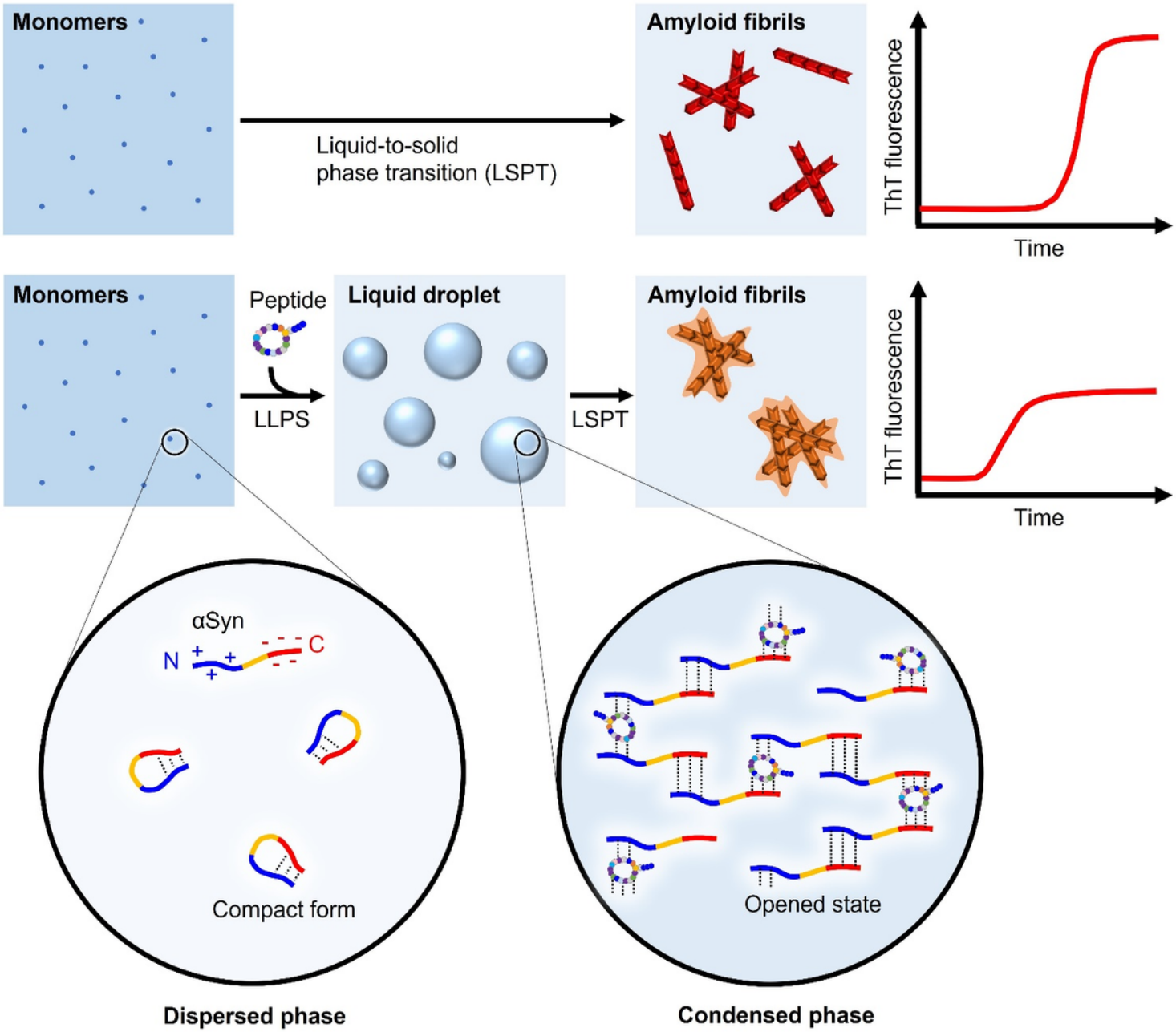

Figure 6

A proposed hypothetical model of αSyn LLPS induced by FL2 and FD1

Under normal physiological conditions, αSyn can form intramolecular interaction between the N- and C-terminal regions. The interaction of FL2 and FD1with the N- and/or C-terminal regions of αSyn may lead to an opened state of αSyn, which is preferred for the formation of an interaction network. Moreover, these peptides can form interactions bridging multiple αSyn molecules, leading to further formation of an interaction network with αSyn and efficient droplet formation. The structural modification of αSyn monomers to an opened state might also accelerate fibril formation, where the exposed NAC region has high amyloid propensity and a N-terminal segment of αSyn (residues 36-42) is required for aggregation.

Supplementary Files

This is a list of supplementary files associated with this preprint. Click to download.

- SupplementaryInformation.pdf
- aSN100NaPiFL210002min.mp4